INT. J. NUM. METH. HEAT FLUID FLOW, VOL. 5, 495–510 (1995)

ON COMPUTATION OF TWO AND THREE-DIMENSIONAL UNSTEADY THERMAL NON-NEWTONIAN FLOWS

D. DING, P. TOWNSEND AND M. F. WEBSTER

University of Wales Institute of non-Newtonian Fluid Mechanics, Department of Computer Science, University of Wales, Swansea, SA2 8PP, U.K.

ABSTRACT

In this article we report on progress in the development of software tools for fluid flow prediction in the polymer processing industry. This involves state-of-the-art numerical techniques and the study of a number of non-trivial model flow problems, in an effort to investigate realistic transient problems relevant to industrial processes. Here we study particularly the effects of variations in non-Newtonian and heat transfer properties of the flowing materials in the flows, both throughout the transient development period and at steady-state.

KEY WORDS Transient Non-Newtonian Non-isothermal Polymers Three dimensions

INTRODUCTION

This work is aimed at developing a computer code to simulate the types of flow which are important in the polymer processing industry. In particular advanced finite element characteristic-based methods for incompressible viscous flows have been implemented for dealing with non-Newtonian materials under transient and non-isothermal conditions. The algorithms used in the code are novel, state-of-the-art and incorporate highly accurate time-stepping integration schemes for the governing differential equations. This involves a combination of Taylor–Galerkin finite element methods with pressure-correction methods. Full details of the mathematics have already been published extensively in the literature[1–5].

We wish to establish confidence in the performance of such a computer code, both in terms of accuracy, and flexibility to deal with a wide range of possible flow conditions and also in terms of its efficiency to compute results. In order to consider these issues with respect to the code referred to above, we have chosen to solve a set of non-trivial model problems. These model problems allow us to investigate the effects on specific flows of varying the non-Newtonian properties and the heat transfer properties of the flowing material. Also the transient capability of the computer code allows the investigation of flow evolution to a steady-state when, for example, temperature boundary conditions are changed impulsively.

In the literature, analytical solutions for steady-state fully developed flows of non-isothermal non-Newtonian fluids have been presented by various authors. Turian[6] presented solutions for planar drag flows between two parallel plates with heat dissipation. This work employed an Arrhenius exponential law for temperature dependence of viscosity and a power-law shear behaviour. Using a perturbation method, solutions were generated for two types of thermal

0961–5539/95/060495–16$2.00

Received January 1994
Revised July 1994

boundary conditions: one with the same temperature applied at both plates and the other with a prescribed temperature at one wall, and a thermally insulated condition at the moving plate. Martin[7] extended this work employing analytical techniques to solve three different problems. This included an axisymmetric pipe flow under a pressure gradient and a fixed wall temperature. Two Couette flows were also solved, under similar temperature boundary condition combinations to Turian, but with a differential in plate temperatures for the prescribed instance. One such flow is a plane shear flow between two parallel plates, and the other is a tangential shear flow between infinite concentric cylinders in relative rotation. Lindt[8] more recently gave a solution for pure drag flow between parallel plates, applicable to the fully developed flow in the metering zone of a screw extruder. He developed an exact solution in the absence of pressure gradients, citing the earlier numerical solutions of Griffith[9] in the presence of pressure gradients, that employed Runge–Kutta numerical integration schemes.

Turning to numerical simulations, steady non-isothermal flows of non-Newtonian polymeric materials have been reported widely. Winter[10] investigated the temperature effect of thermal power-law fluids in two dimensional extruder dies under various boundary conditions. The momentum and the energy equations were solved based on a decoupled finite difference method. It was shown that viscous heating created an increase of the temperature in the die. These results agree well with our two-dimensional studies. Mitsoulis *et al.*[11] presented a high speed wire-coating problem for polyethylene with shear rate and temperature-dependent viscosity under complex boundary conditions. A finite element method was employed to solve the momentum and energy equations using a decoupled scheme. Effects of viscous dissipation were also found in the temperature field and the non-isothermal predictions gave better predictions than the isothermal analysis. Karagiannis *et al.*[12] studied extrusion problems of non-isothermal Newtonian flow through a straight three-dimensional die with a square cross section, employing a finite element approach. Isothermal boundary conditions were applied to the die walls and viscous heating effects were observed. These solutions are in general agreement with our own for a similar three-dimensional thermal flow in a curved channel of square cross section for a non-Newtonian fluid. We are not aware of any available data against which to compare our transient analysis.

In this paper the results of simulations for a number of different flow conditions and geometries are presented. Velocity and temperature profiles are given, both for the final steady-state and for stages throughout the flow evolution. The influence on such profiles of the non-Newtonian power-law index m on the viscous heating generated is considered as well as the effect of variation in the material constant β, a thermal exponential factor. It is shown that the algorithms involved perform well under a variety of conditions, giving confidence in results predicted for other flows for which no analytical solution is available, or for which it is not possible to obtain experimental measurements. The range of problems discussed are of varying complexity. These include problems where a transient phase is significant to those where only the steady-state is relevant, and cover various instances of Couette and Poiseulle flows with a variety of thermal boundary and initial conditions imposed. Instances of problems in both two and three dimensions are considered. Reference is made to an earlier study[3], where Couette flows are cited for comparison against available analytical solutions (see also reference 5 in the unsteady context). This formed a basis from which to develop the work presented here where analytical solutions are not readily available.

The numerical algorithms we are currently developing within a general purpose software suite to address different materials and flow types. Examples of these lie within glass flow, fibre suspension flow, visco-elastic flow, capillary flow and multi-layer injection moulding. For multi-layer injection moulding we are studying fully three dimensional problems for complex shaped moulds and this work involves tracking material deformation and moving flow fronts. In a separate project the simulation software has been interfaced to a commercially available CAD/CAM package and a visualisation package, and it is envisaged that this will provide ultimately a general purpose software tool of wide ranging application in non-Newtonian computational fluid dynamics, of particular value for polymer processing.

DESCRIPTION OF MODEL PROBLEMS

In Reference 3 four model problems were addressed, three Couette flows and one Poiseuille flow. For the instances of Couette flow, the effects of a temperature dependent viscosity were considered and compared against steady-state analytic solutions. Then a power-law shear-thinning functionality was incorporated into the viscosity to extend consideration to generalised Newtonian fluids. Again analytic comparisons were to hand and excellent agreement was achieved with the numerical solutions obtained for power-law index $0.2 \leqslant m \leqslant 1.0$. Subsequently two transient problems were solved, one of a Couette and the other of a Poiseuille flow. Some interesting transient phenomena were reported in the temperature fields with variation in m and thermal Péclet number. At the chosen level of $\beta = 1$ and for a fixed value of m, there was little noticeable effect on the velocity fields from the corresponding isothermal profiles. It is therefore to this issue that present attention is drawn by altering β, as well as additional variation with m and the imposition of realistic initial and boundary conditions to the problems studied. Here two Poiseuille flows are studied which incorporate a wide variation in shear-rate and are capable therefore of manifesting significant field effects.

The particular geometry under study is that of a two-dimensional plane channel of one unit width and ten units length. This domain is discretised uniformly according to Reference 3, using some 200 triangular finite elements where a pair of such elements subdivide a rectangle of side 0.1*1.0 units. The interpolation functions used are piecewise continuous quadratics for velocities and temperature, and linear for pressure. This implies a total number of nodal unknowns of 441 for each velocity component and temperature, and 121 for pressure. The numerical parameters chosen follow Reference 3 with typically, time-step of $\Delta t = 10^{-2}$ and time-stepping convergence tolerance of 10^{-4}. Three Jacobi iterations are used per fractional solution stage, for both full and half time step momentum equation stages, and at the end of time step divergence-free velocity recovery stage.

The first transient problem studied follows problem 4 of Reference 3 a thermal Poiseuille flow problem with constant temperature boundary conditions and a unit flowrate that develops under viscous heating. The thermal Péclet number adopted is unity and in the present context this problem is referred to as Poiseuille problem A. The effects of an increased thermal factor from $\beta = 1$ to $\beta = 5$ are considered. The initial conditions are taken as the Newtonian isothermal equivalent conditions, and to achieve a physically realistic transient inlet boundary condition some attempt is made to recycle the exit flow conditions back to the inlet at certain well-chosen times in the development of the flow. This has the effect of continually looking down a longer and longer geometry and effectively simulates the imposition of periodic boundary conditions. A final test to this procedure is to take the ultimate solution and recompute such a problem with the entry condition fixed to confirm the correctness of this solution, which has been demonstrated in all instances tested.

A second transient problem considered here is that of a thermal Poiseuille flow problem of unit flowrate that develops under viscous heating when there is a sudden increase in temperature boundary condition on the second half only of the channel walls. Again, the thermal Péclet number is taken as unity and this problem is referred to as Poiseuille problem B, shown schematically in *Figure 1*. The temperature boundary condition applied initially obeys a step function and the initial conditions are those adopted from problem A above, being both generalised Newtonian and non-isothermal as appropriate. This problem closely approximates industrially realisable conditions, perhaps only to be superseded by adopting a more gradually changing function for the wall boundary condition on temperature. Consideration is given again here to the influence of variation in the power-law index and change in β from 1 to 5.

A third problem considered is that of non-isothermal non-Newtonian pressure-driven flow around a curved channel of square cross section, where we focus attention on steady-state solutions. This problem exhibits fully three-dimensional effects, and its isothermal Newtonian counterpart was investigated in an earlier publication[13]. *Figure 2* shows a plan view of the

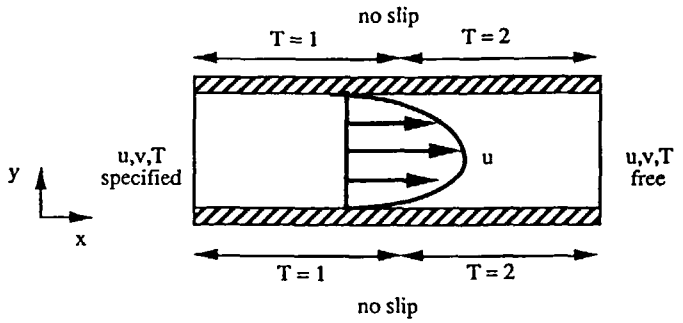

Figure 1 Schematic diagram for Poiseuille problem B

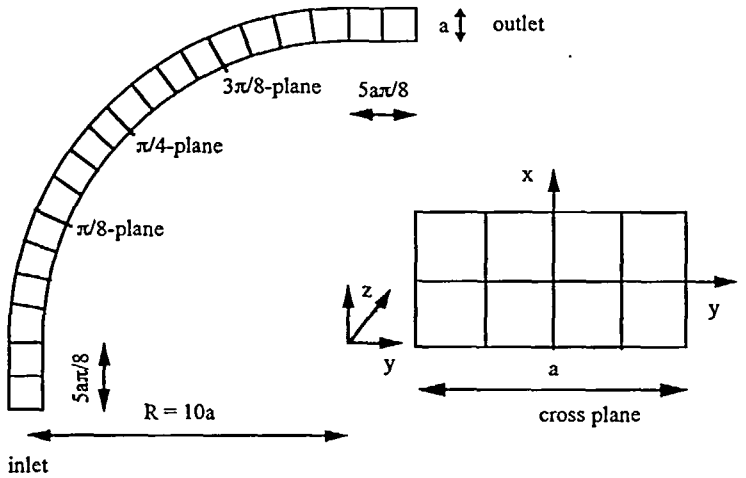

Figure 2 Plan view of 3-D problem

geometry, where a channel with square cross section is curved through 90° and straight channel sections are added at both inlet and outlet regions. Adopting symmetry assumptions only the upper half of the channel is considered in the simulations. Cross flow components are set to zero on both entry and exit stations. A fully developed axial velocity profile for a straight pipe with square cross section is applied at the inlet, and a normal traction free condition is imposed at the outlet. Temperature boundary conditions are prescribed as unitary on the wall and the inlet, and taken as insulated elsewhere. A thermal Carreau–Yasuda model is selected as the constitutive model to describe the viscosity behaviour.

THEORETICAL CONSIDERATIONS

The present version of the algorithm follows closely that which has already appeared in the literature cf. 1–4. The purpose here is to direct specific attention to those key areas where changes arise. For example, here there is a specific requirement to accommodate a generalised Newtonian non-isothermal fluid prescription and as such the viscosity function is assumed to behave according to a power-law model,

$$\mu = \mu_o \dot{\gamma}^{m-1} e^{-\beta(T-T_o)} \tag{1}$$

for some two-dimensional problems, where μ_o is the viscosity at the reference temperature T_o

and reference shear rate of unity, $\gamma = 0.5(\mathrm{I}_2)^{1/2}$ for the second invariant I_2 of the rate of strain tensor (see Reference 7 for definition), m is the power-law index, T is the fluid temperature and β is a material constant. A Carreau–Yasuda model is also employed for a three-dimensional problem as,

$$\mu = \{\mu_\infty + (\mu_o - \mu_\infty)[1 + (\lambda\dot{\gamma})^2]^{\frac{m-1}{2}}\} e^{-\beta(T-T_o)} \tag{2}$$

where μ_o is the viscosity at the reference temperature T_o and vanishing shear rate, μ_∞ is an asymptotic value of viscosity at very high shear rate and λ is a material constant.

In computations, the following non-dimensionalised scheme is adopted,

$$\mathbf{x}^* = \frac{x}{L}, \mathbf{u}^* = \frac{u}{V}, T^* = \frac{T}{T_o}, \mu^* = \frac{\mu}{\mu_c} \tag{3}$$

where L, V, T_o and μ_c are characteristic length, velocity, temperature and viscosity respectively. We take L to be the width of the channel, V to be the maximum fluid velocity at the inlet, T_o to be 1 K, μ_c to be 1 Pa s. This leads to the definition of two dimensionless groups, $Re = \dfrac{\rho LV}{\mu_c}$ and $Pe = \dfrac{c_p LV}{\kappa}$, where ρ is fluid density, κ is thermal conductivity and c_p is heat capacity at constant pressure. Discarding the * notation for brevity, the dimensionless parameters involved in the power-law case are $\mu_0 = 1$, $m = 1$, 0.2, $\beta = 1$, 5, and in the Carreau–Yasuda model $\mu_0 = 10$, $\mu_\infty = 0.01$ and $\lambda = 8$ (given in Reference 14), $m = 0.2$, $\beta = 5$.

A Taylor–Galerkin algorithm is employed to solve the governing equations relating to the conservation of mass, momentum and energy. A time stepping scheme is derived through Taylor series expansions up to second order in time step and a two-step predictor-corrector scheme is assumed. This, in conjunction with a pressure correction method to accommodate the incompressibility constraint, produces a fractional staged equation system to solve of three distinct phases on each time step. A semi-implicit treatment of a Crank-Nicolson type is adopted for diffusion terms and the energy equation is taken identically to the momentum equation over the first solution phase. A Galerkin finite element spatial discretisation renders a fully discrete system with the choice of piecewise continuous quadratics (ϕ) for velocity and temperature, and linears for pressure (ψ). This system is outlined for completeness, employing the following notation where superscripts denote the time level. $\mathbf{U}^n$ is a nodel velocity vector, $\mathbf{U}^*$ is an intermediate nondivergence-free velocity vector, $\mathbf{T}^n$ is a temperature vector, $\mathbf{P}^n$ is a pressure vector, $\mathbf{Q}^{n+1} = \mathbf{P}^{n+1} - \mathbf{P}^n$ is the pressure difference vector and $\mathbf{F}^n$ is a forcing function vector due to imposed boundary conditions on boundary segment Γ of spatial domain Ω (see References 1, 13). Our system is specified as,

1a:
$$\left[\frac{2\rho}{\Delta t}\mathbf{M} + \frac{1}{2}\mathbf{S}_u\right](\mathbf{U}^{n+\frac{1}{2}} - \mathbf{U}^n) = \frac{1}{2}(\mathbf{F}^n + \mathbf{F}^{n+\frac{1}{2}}) + \{-[\mathbf{S}_u\mathbf{U} + \rho\mathbf{N}(\mathbf{U})\mathbf{U}] + \mathbf{L}\dagger\mathbf{P}\}^n, \tag{4}$$

$$\left[\frac{2\rho c_p}{\Delta t}\mathbf{M} + \frac{1}{2}\mathbf{S}_T\right](\mathbf{T}^{n+\frac{1}{2}} - \mathbf{T}^n) = \frac{1}{2}(\mathbf{F}^n + \mathbf{F}^{n+\frac{1}{2}}) + \{-[\mathbf{S}_T\mathbf{T} + \rho c_p\mathbf{N}(\mathbf{U})\mathbf{T}] + \mu\Phi(\mathbf{U})\}^n, \tag{5}$$

1b:
$$\left[\frac{\rho}{\Delta t}\mathbf{M} + \frac{1}{2}\mathbf{S}_u\right](\mathbf{U}^* - \mathbf{U}^n) = \frac{1}{2}(\mathbf{F}^n + \mathbf{F}^{n+1}) + [-\mathbf{S}_u\mathbf{U} + \mathbf{L}\dagger\mathbf{P}]^n - [\rho\mathbf{N}(\mathbf{U})\mathbf{U}]^{n+\frac{1}{2}}, \tag{6}$$

$$\left[\frac{\rho c_p}{\Delta t}\mathbf{M} + \frac{1}{2}\mathbf{S}_T\right](\mathbf{T}^{n+1} - \mathbf{T}^n) = \frac{1}{2}(\mathbf{F}^n + \mathbf{F}^{n+1}) - \mathbf{S}_T\mathbf{T}^n + [-\rho c_p\mathbf{N}(\mathbf{U})\mathbf{T} + \mu\Phi(\mathbf{U})]^{n+\frac{1}{2}}, \tag{7}$$

2: $$\frac{1}{2}\mathbf{K}\mathbf{Q}^{n+1} = -\frac{\rho}{\Delta t}\mathbf{L}\mathbf{U}^{*}, \tag{8}$$

3: $$\frac{\rho}{\Delta t}\mathbf{M}(\mathbf{U}^{n+1} - \mathbf{U}^{*}) = \frac{1}{2}\mathbf{L}\dagger\mathbf{Q}^{n+1}, \tag{9}$$

where matrix transpose is denoted by †, repeated indices implies summation, and associated matrix and vector notation is taken as

$$\mathbf{M}_{ij} = \int_{\Omega} \phi_i \phi_j \mathrm{d}\Omega,$$

$$\mathbf{N}_{ij}(\mathbf{U}) = \int_{\Omega} \phi_i \left(U_k^l \phi_l \frac{\partial \phi_j}{\partial x_k} \right) \mathrm{d}\Omega,$$

$$\mathbf{K}_{ij} = \int_{\Omega} \nabla\psi_i \cdot \nabla\psi_j \mathrm{d}\Omega,$$

$$(\mathbf{L}_k)_{ij} = \int_{\Omega} \psi_i \nabla_k \phi_j \mathrm{d}\Omega,$$

$$(\mathbf{S}_u)_{ij} = (\mathbf{S}_{lm})_{ij},$$

$$(\mathbf{S}_T)_{ij} = \kappa \int_{\Omega} \nabla\phi_i \cdot \nabla\phi_j \mathrm{d}\Omega.$$

The dissipation vector is given by,

$$\Phi_i = \frac{1}{2}\int_{\Omega} \mu\phi_i \left(\frac{\partial \phi_m}{\partial x_k} U_l^m + \frac{\partial \phi_m}{\partial x_l} U_k^m \right)^2 \mathrm{d}\Omega, \qquad k,l = 1,2,3$$

where x_1, x_2 and x_3 indicate Cartesian coordinates and,

$$\nabla\phi_i = \left(\frac{\partial \phi_i}{\partial \mathrm{x}}, \frac{\partial \phi_i}{\partial \mathrm{y}}, \frac{\partial \phi_i}{\partial \mathrm{z}} \right)^{\dagger},$$

$$(S_{lm})_{ij} = \left[\int_{\Omega} \mu \left\{ \chi_{lk} \frac{\partial \phi_i}{\partial x_k} \frac{\partial \phi_j}{\partial x_k} \right\} \mathrm{d}\Omega \right] \qquad \text{if } l = m,$$

$$(S_{lm})_{ij} = \left[\int_{\Omega} \mu \left\{ \frac{\partial \phi_i}{\partial x_m} \frac{\partial \phi_j}{\partial x_l} \right\} \mathrm{d}\Omega \right] \qquad \text{if } l \neq m,$$

$$\chi_{lk} = 2 \text{ if } l = k \text{ and } 1 \text{ if } l \neq k \text{ where } l,m,k = 1,2,3.$$

The first solution phase involves a half time step predicted solution for both velocity and temperature, prior to a correction to obtain a full time step non-divergence free velocity field and associated temperature. These equations are solved by a Jacobi iteration. The second solution phase requires the calculation for the pressure difference on the time step according to a Poisson equation with source dependency on the velocity solution of phase one. This subproblem is solved by a direct Choleski method. The third and final solution phase is instigated to provide the divergence free velocity at the end of the time step to second order accuracy. Again Jacobi iteration is used for this stage. A virtue of the algorithm is that it does not generate large system matrices. This is a significant advantage when dealing with large scale or geometrically complex problem and, in particular, for dealing with three-dimensional problems.

Treatment of the generalised momentum equations involves consideration of the diffusion in terms of the rate of strain tensor D (see Reference 1 for more detail). Under the semi-implicit Taylor–Galerkin formulation of Reference 4 this leads to a full (as opposed to a diagonal)

subsystem matrix for the momentum component equations. The viscosity μ in momentum diffusion matrix S_u is evaluated at an appropriate time level using the most recent known velocity and temperature fields. It follows directly that the generalised momentum subsystem matrix is symmetric positive definite. This can be observed from the fact that for any nonzero vector U, diffusion subsystem matrix $[S_u]$ and viscous dissipation function Φ,

$$\mathbf{U}^T[\mathbf{S}_u]\mathbf{U} = \int_\Omega \mu\{\Phi\}\mathrm{d}\Omega, \tag{10}$$

which is non-negative as $\Phi \geqslant 0$ by definition and μ is a positive function. This property underpins the iterative solution procedure that is implemented at stages 1 and 3 of the fractional stage scheme reported earlier. The Jacobi nature of this iteration with its diagonalised preconditioning matrix and the element-wise construction for matrix-vector products in the right-hand side vectors do not alter from those cited in References 3, 4. However, the velocity solution components are now coupled together in the right-hand side products, and quadrature is necessary to capture accurately the spatial dependency of the variable viscosity function and the diagonalised preconditioner is now itself time-dependent.

It is worth pointing out that a variation to the above scheme with the diffusion subsystem matrix split into diagonal and off-diagonal component sections has also been considered. The diagonal section was treated in a Crank–Nicolson implicit manner and the off-diagonal section dealt with via the explicit Taylor–Galerkin predictor-corrector approach using a half time-step. Such a partially implicit treatment of the diffusion terms was found to yield, as expected, a less stable scheme which became apparent when studying a Couette flow problem due to Turian and Bird[15] with a temperature dependent viscosity. Such an alternative, less costly scheme is certainly not to be advocated here therefore.

SIMULATION RESULTS

Poiseuille problem A

Many aspects of this problem were discussed in a previous article[3], where an attempt was made to predict velocity and temperature development for a range of material parameters. In the work described here we investigate further the effect of temperature variations on the flow field. The temperature within the fluid changes with time as a result of viscous heating, and provided one has sufficiently sensitive material parameter settings, this change in temperature feeds back to modify the velocity profile. The latter, of course, also changes as a result of shear-thinning. One might argue that the boundary conditions used in Reference 3 were somewhat artificial and it is certainly true that they did not represent any truly physical transient behaviour. However one can obtain a more realistic steady-state by integrating the above problem to convergence and then feeding back the converged outlet profiles for velocity and temperature as new inlet conditions. This procedure is adopted in this paper but in practice, apart from the inlet conditions themselves, this proves to have little or no effect on the remainder of the flow region. Thus it is shown that fully-developed non-Newtonian Poiseuille flow had emerged very rapidly only a short distance downstream of the imposed isothermal Newtonian inlet flow.

In *Figure 3*, converged steady-state (css) velocity profiles are given for different values of m and β, where the annotation follows that used in *Figure 5*. Outlet profiles only are displayed as there are no significant changes observed over the channel length. If we first consider the effect of shear-thinning as illustrated by curves (a) and (b), it can be seen that for values of m less than unity a significantly flatter profile is obtained with a boundary layer behaviour near the walls where the viscosity of the sheared fluid is greatly reduced. If we compare curves (a) and (c), where in both cases $m = 1$, i.e. no shear-thinning, we can isolate the effect of the change in the thermal parameter β. For $\beta = 1$ there is little or no feed-back of viscous heating into the velocity profile which remains essentially the same as a Newtonian parabolic profile. When β is increased

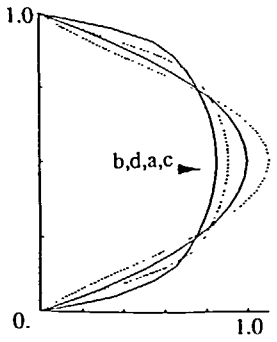

Figure 3 Exit profiles for velocity

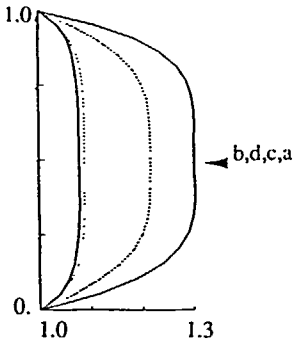

Figure 4 Exit profiles for temperature

to 5, however, a significant change takes place. The small temperature rise in the fluid lying midway between the bounding channel walls is sufficient to reduce the viscosity to such an extent that the fluid in this region moves more rapidly and one sees developing a characteristic bell-shaped velocity profile. If one combines both shear-thinning and thermal effects, a compromise profile, as shown in curve (d), develops. *Figure 4* shows the corresponding temperature profiles for the four different cases. A comparison of curve (a) with (b) and (c) shows that the reduction in viscosity due to either shear-thinning or increased temperature feed-back has the effect of reducing the viscous heating in the fluid. From curve (d) it is seen that when both influences are taken into account, however, they do not reinforce one another, but rather an intermediate profile is achieved. *Figures 5* and *6* summarise the transient development to a steady-state of the velocity and temperature channel exit profiles respectively. For the velocity there is a gradual change from the Newtonian profile, whilst for the temperature one sees a characteristic increase in temperature in the high shear regions near the walls which eventually diffuses into the remainder of the fluid to give a flat-topped steady-state temperature profile.

The temperature profiles of Winter[10], as they develop down the die for a thermal power-law fluid under isothermal boundary conditions, bear out our results shown in *Figures 6b* and *6c*. It is found that the temperature at the wall region increases more than that at the centre of the channel due to viscous dissipation, and radial heat conduction balances the dissipation. This leads to the observed fully developed temperature field at the flow outlet.

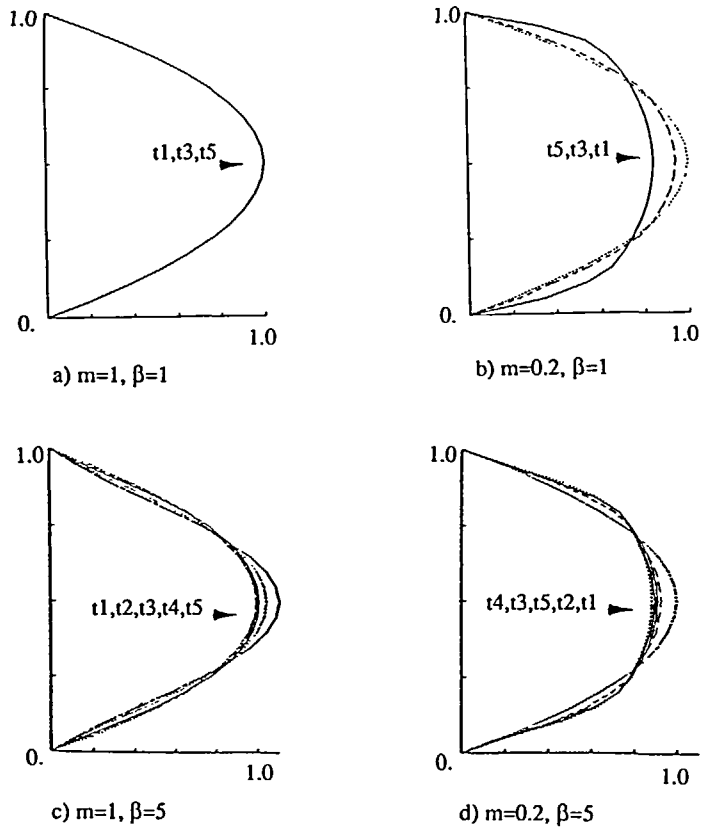

Figure 5 Exit profiles for velocity (t1 = 0, t2 = 0.1, t3 = 0.2, t4 = 0.5, t5 = css)

Poiseuille problem B

For reasons outlined earlier, the Poiseuille problem A represented somewhat artificial flow conditions. In an attempt to simulate a more realistic start up, a similar problem has been solved with a set of initial and boundary conditions as outlined previously, and is designated Poiseuille problem B. For this problem the converged steady-state developed in Poiseuille problem A is taken as the starting field for both velocity and temperature, and also an instantaneous step change in the temperature is made to the downstream halves of the boundary channel walls (see figure 1). Here an identical characteristic velocity μ_o of unity is employed for both Newtonian and non-Newtonian flows.

Figures 7 and *8* show the velocity and temperature development in space and time for various material parameter settings. For $\beta = 1$ the feed-back of temperature rise into the momentum equations is of such little consequence that no discernible change from the inlet velocity profile is apparent. For this reason these plots have been omitted. For $\beta = 5$, however, the feed-back of temperature rise into the momentum equations does effect velocity profiles. *Figures 7(a)* and *7(b)* show the velocity development for $m = 1$ and $m = 0.2$ respectively. Velocity profiles flatten compared with $\beta = 1$, as larger β leads to less viscous heating for a fixed value of m. Shear-thinning again causes flatter velocity profiles. *Figure 8(a)* shows the temperature development for $m = 1$ and $\beta = 1$. The instantaneous increase in temperature at the walls in the right half of the flow

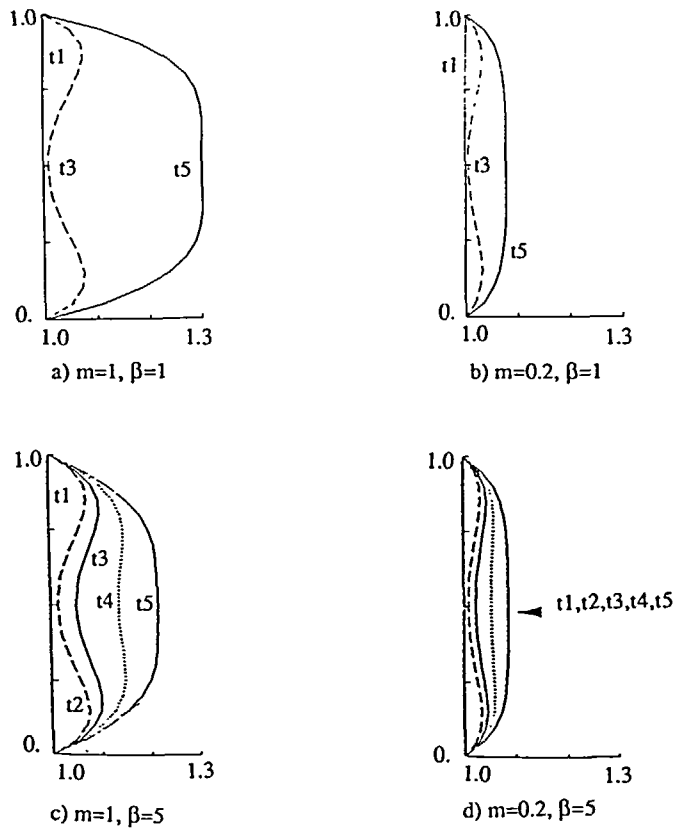

Figure 6 Exit profiles for temperature (t1 = 0, t2 = 0.1, t3 = 0.2, t4 = 0.5, t5 = css)

region is seen to gradually diffuse in time until one obtains the same profile as at the inlet but offset by the step change in temperature. *Figure 8(b)* shows the effect of shear-thinning, where the pattern of development is essentially the same as for *Figure 8(a)*. The same behaviour is observed in *Figures 8(c)* and *8(d)* for $\beta = 5$, but the thermal viscous contribution is reduced from that in *Figures 8(a)* and *8(b)*.

Thermal three-dimensional problem

Here we concentrate on steady solutions for this three-dimensional non-Newtonian thermal flow, illustrating the effects of viscous dissipation and heat transfer under isothermal channel boundary conditions. This involves a Carreau–Yasuda model and values of inertia of $Re = 1$ and 100 are considered. *Figure 9* shows steady-state dimensionless axial velocity profiles for $Re = 1$ and 100 on the horizontal symmetrical midplane of the geometry at three stations $\pi/8$, $\pi/4$ and $3\pi/8$ around the bend. The cross-field velocity vector plots for $Re = 100$ are also displayed at the same stations around the bend. In the axial velocity profile plots, the zero position on the horizontal axis indicates the outer wall of the bend and unity indicates the inner wall of the bend. It is observed that the fluid near the outer wall moves faster than that near the inner wall for the $Re = 100$ case, and secondary flow is apparent on the vertical cross-planes around the

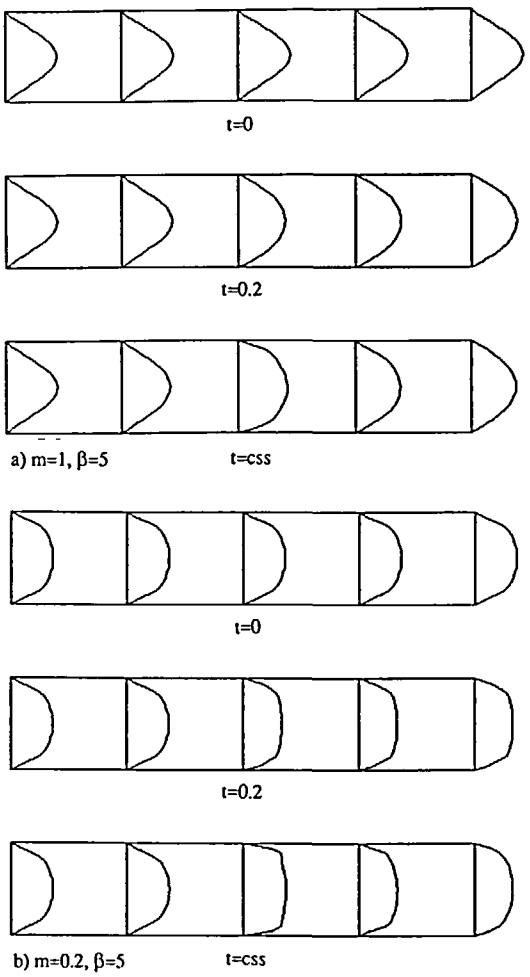

Figure 7 Velocity profiles along the mesh

bend at the stations monitored. This is not observed for the lower value of inertia of $Re=1$, where the fluid moves more slowly.

Figure 10 shows steady state midplane dimensionless temperature profiles as the fluid travels around the bend for values of $Re=1$ and 100, equivalent to thermal Péclet numbers of $Pe=1$ and 100 respectively. A number of observations may be made. First, the fluid temperature rises due to viscous heating. Second, the temperature increase in the flow domain for $Re=100$ is much less than that for $Re=1$, as the higher level of Pe reduces heat dissipation. Third, for $Re=100$, the fluid near the wall is hotter than that in the core flow, since high Pe reduces the level of heat diffusion and amplifies heat convection in the axial direction. Lastly for $Re=100$, the fluid in the outer wall vicinity is hotter than that near the inner wall, because larger shear rates are experienced in the outer wall region (cf. *Figure 9*). This inertial picture was also observed in the Newtonian isothermal equivalent studies[13].

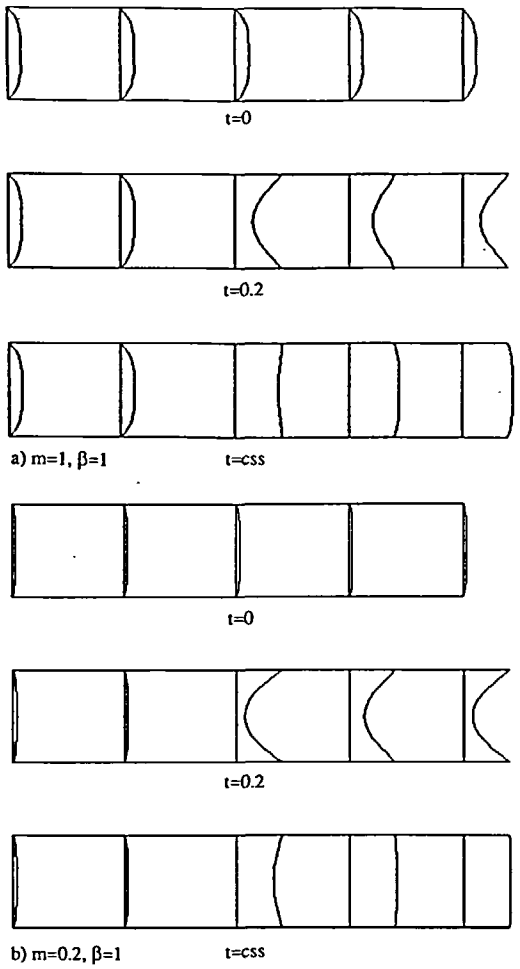

Figure 8 Temperature profiles along the mesh

Karagiannis *et al.*[12] studied a similar three-dimensional thermal problem, of pressure-driven flow of a Newtonian fluid down a straight pipe of square cross-section. These authors produced solutions under creeping flow ($Re=(10^{-6})$) for isothermal boundary conditions and taking viscous dissipation into account. Their thermal Newtonian steady solution is broadly in agreement with our own results, taking into account the previous arguments, where we observe the reduction in the level of viscous heating due to reduction in power-law index. For the higher level of inertia of $Re=100$, due to asymmetry generated in the axial velocity profiles caused by the bending in the geometry (cf. *Figure 9*), we observe asymmetry in the cross-flow temperature profiles. Peak temperatures arise near the walls, with a maximum occurring near the outer wall, and this gives cooler core flow than in the vicinity of the wall.

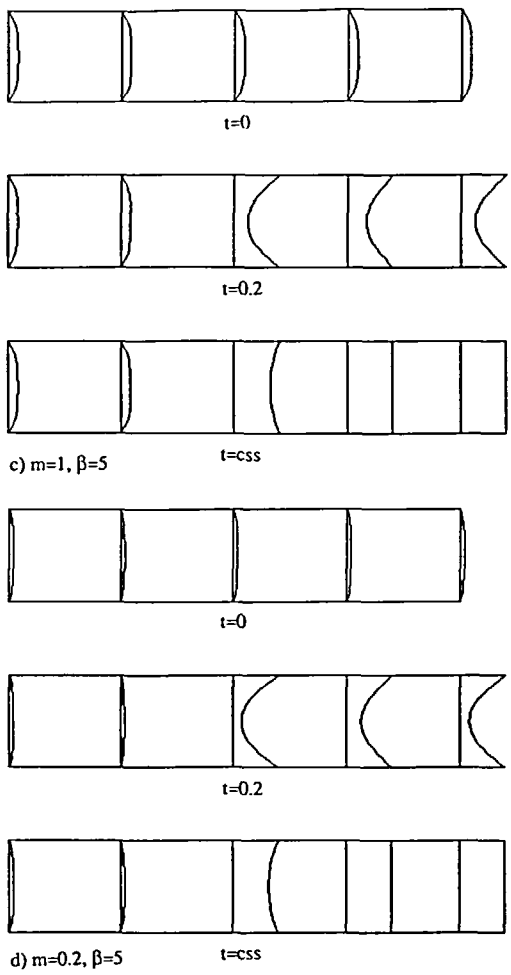

Figure 8 Temperature profiles along the mesh

CONCLUSIONS

In this paper progress in the development of software tools for fluid flow prediction relevant to the polymer processing industry has been reported. In particular the nonlinear effect of viscous heating coupled with variations in viscosity of the flowing materials due to shear and temperature changes has been studied, both throughout the transient development period and at steady-state. The work presented forms part of a phased evaluation of the software tools for model problems, although the capabilities of the software are quite general, as illustrated by the inclusion of a complex three-dimensional example. The results reported have demonstrated significant effects within the flow fields for these problems at the material parameters selected. The influence of shear and temperature change on the fluid viscosity may produce either contra or like effects, although when both are present a combination of the individual effects takes place. For Poiseuille problem B a sudden change in wall temperature brought about significant changes to the velocity

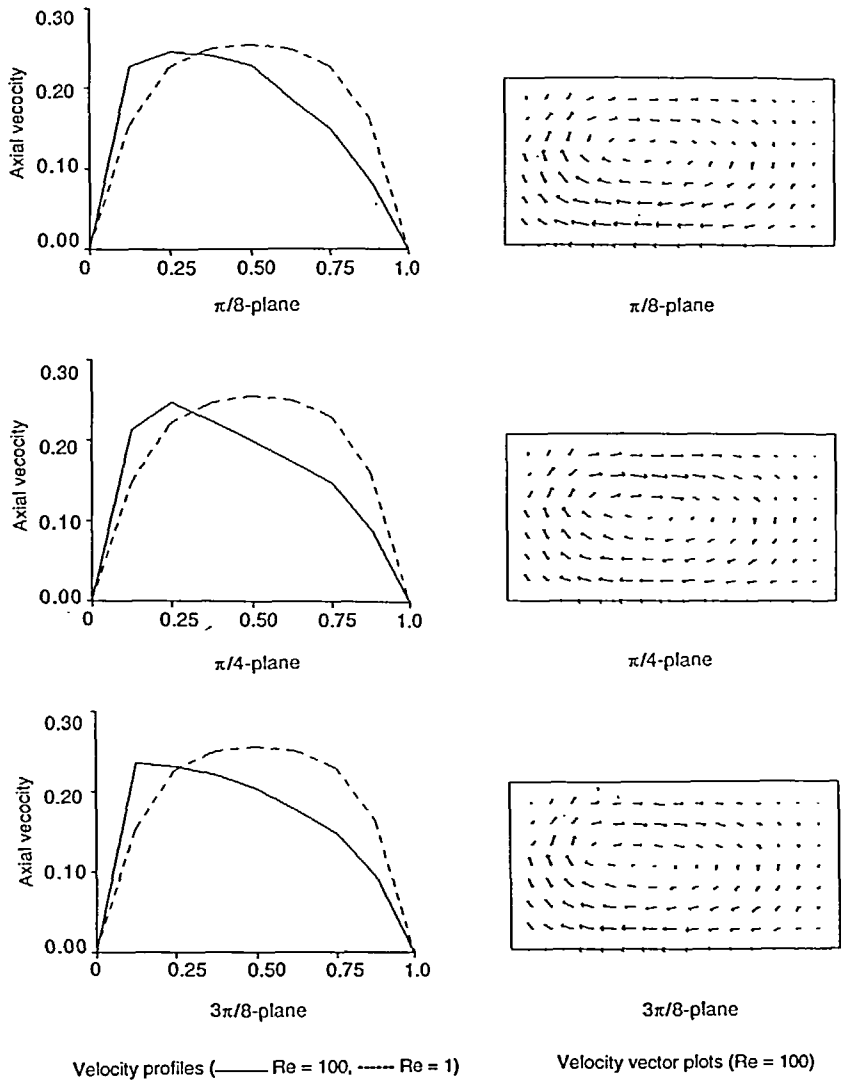

Figure 9 Axial velocity profiles and cross field vector plots (Carreau–Yasuda model, $m=0.2$, $\beta=5$)

profile upstream of the hotter portion of the channel walls. For the three-dimensional problem, larger values of inertia (and thermal Péclet number) of the order 100 not only distort the symmetry of the axial velocity profiles, but also that in the temperature profiles over the geometry horizontal midplane. This results in less heat diffusion than for lower values of inertia of the order of unity.

REFERENCES

1 Townsend, P. and Webster, M. F. An algorithm for the three-dimensional transient simulation of non-Newtonian fluid flow, *Transient/Dynamic Analysis and Constitutive Laws for Eng. Materials*, Eds G. N. Pandé and J. Middleton, Nijhoff (1987)

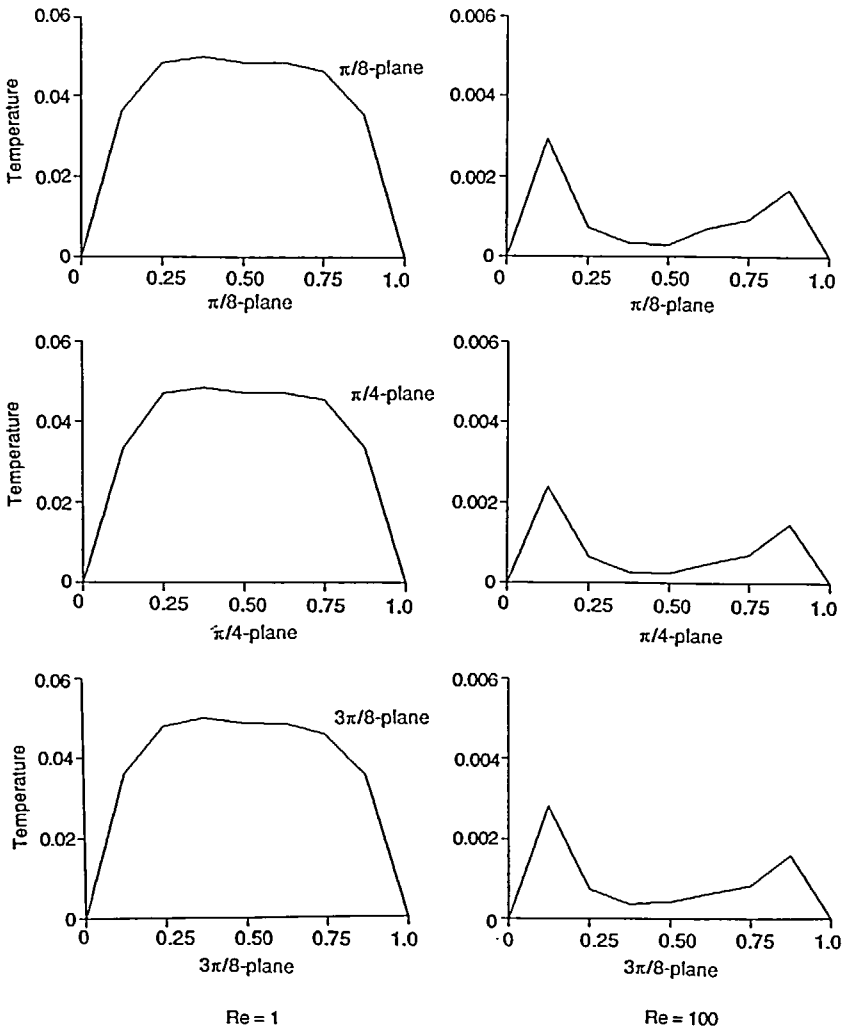

Figure 10 Axial temperature profiles (Carreau–Yasuda model, m = 0.2, $\beta = 5$)

2 Webster, M. F. and Townsend, P. Development of a transient approach to simulate Newtonian and non-Newtonian flow, *Num. Meth. in Eng.: Theory and Applications*, Eds G. N. Pandé and J. Middleton, Elsevier Applied Science (1990)
3 Ding, D., Townsend, P. and Webster, M. F. The development of flow simulation software for polymer processing applications, *Rev. Port. Hemorreologia*, **4**, Suppl.1/Pt A, 31-38 (1990)
4 Hawken, D. M., Tamaddon-Jahromi, H. R., Townsend, P. and Webster, M. F. A Taylor-Galerkin based algorithm for viscous incompressible flow, *Int. J. Num. Meth. Fluids*, **10** (3), 327–351 (1990)
5 Tamaddon-Jahromi, H. R., Townsend, P. and Webster, M. F. Numerical solution of unsteady viscous flows, *Comp. Meth. Appl. Mech. Eng.*, **95**, 301–315 (1992)
6 Turian, R. M. Viscous heating in the cone-and-plate viscometer—III. Non-Newtonian fluids with temperature-dependent viscosity and thermal conductivity, *Chem. Eng. Sci.*, **20**, 771–781 (1965)
7 Martin, B. Some analytical solutions for viscometric flows of power-law fluids with heat generation and temperature dependent viscosity, *Int. J. Non-linear Mechanics*, **2** (4), 285–301 (1967)
8 Lindt, L. T. Flow of a temperature dependent power-law model fluid between parallel plates: an approximation for flow in a screw extruder, *Polym. Eng. Sci.*, **29** (7), 471–478 (1989)

9 Griffith, R. M. Fully developed flow in screw extruders, *Ind. Eng. Chem. Fundam.*, **1**, 180–187 (1962)
10 Winter, H. H. Temperature fields in extruder dies with circular annular or slit cross-section, *Polym. Eng. Sci.*, **15** (2), 84–89 (1975)
11 Mitsoulis, E., Wagner, R. and Heng, F. L. Numerical simulation of wire-coating low-density polyethylene: theory and experiments, *Polym. Eng. Sci.*, **28** (5), 291–310 (1988)
12 Karagiannis, A., Hrymak, A. N. and Vlachopoulos, J. Three-dimensional extrusion flows, *Rheologica Acta*, **28** (2), 121–133 (1989)
13 Hassager, O., Henriksen, P., Townsend, P., Webster, M. F. and Ding, D. The quarterbend: a three-dimensional benchmark problem, *J. Comput. Fluids*, **20** (4), 373–386 (1991)
14 Obaid, T. S. and Townsend, P. A computer model of the two-roll mill for generalised Newtonian flow, *Rheologica Acta*, **23**, 255–260 (1984)
15 Turian, R. M. and Bird, R. B. Viscous heating in the cone-and-plate viscometer—II. Newtonian fluids with temperature-dependent viscosity and thermal conductivity, *Chem. Eng. Sci.*, **8**, 689–696 (1963)